Supplemental Materials for

Tetragonal Mexican-Hat Dispersion and Switchable Half-Metal State with Multiple Anisotropic Weyl Fermions in Penta-Graphene

Ningning Jia[1], Yongting Shi[1], Zhiheng Lv[1], Junting Qin[1], Jiangtao Cai[2], Xue Jiang[3], Jijun Zhao[3*], Zhifeng Liu[1*]

[1]*Key Laboratory of Nanoscience and Nanotechnology, School of Physical Science and Technology, Inner Mongolia University, Hohhot 010021, China*

[2]*Department of Physics, Shaanxi University of Science and Technology, Xi'an 710021, China*

[3]*Key Laboratory of Materials Modification by Laser, Ion and Electron Beams (Dalian University of Technology), Ministry of Education, Dalian 116024, China*

Table of Contents

*zhaojj@dlut.edu.cn (J. Zhao); zfliu@imu.edu.cn (Z. Liu)

I. Electronic band structures from HSE06

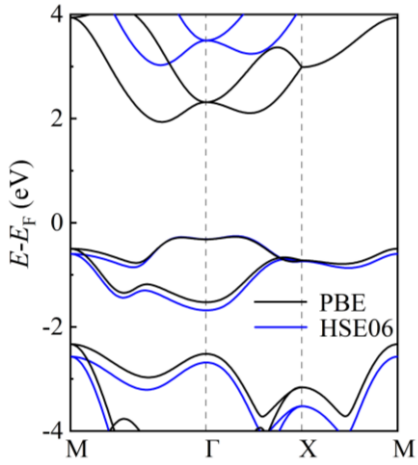

FIG. S1. The electronic band structures of penta-graphene calculated by HSE06 (blue solid line). For comparison, the bands (black solid line) from PBE are also presented. Clearly, the two methods can give the same results for the studied Mexican-hat valence band.

II. Spin-polarized charge densities of different magnetic states

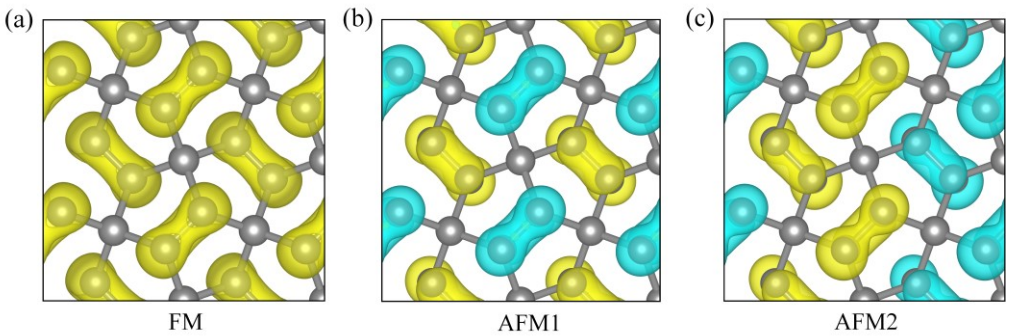

FIG. S2. The spatial distribution of spin-polarized charge density for penta-graphene at the density of 7.36 $\times 10^{14}$ cm^{-2} in possible magnetic configurations: (a) FM, (b) AFM1 and (c) AFM2.

III. The Curie temperature under different hole-doping densities

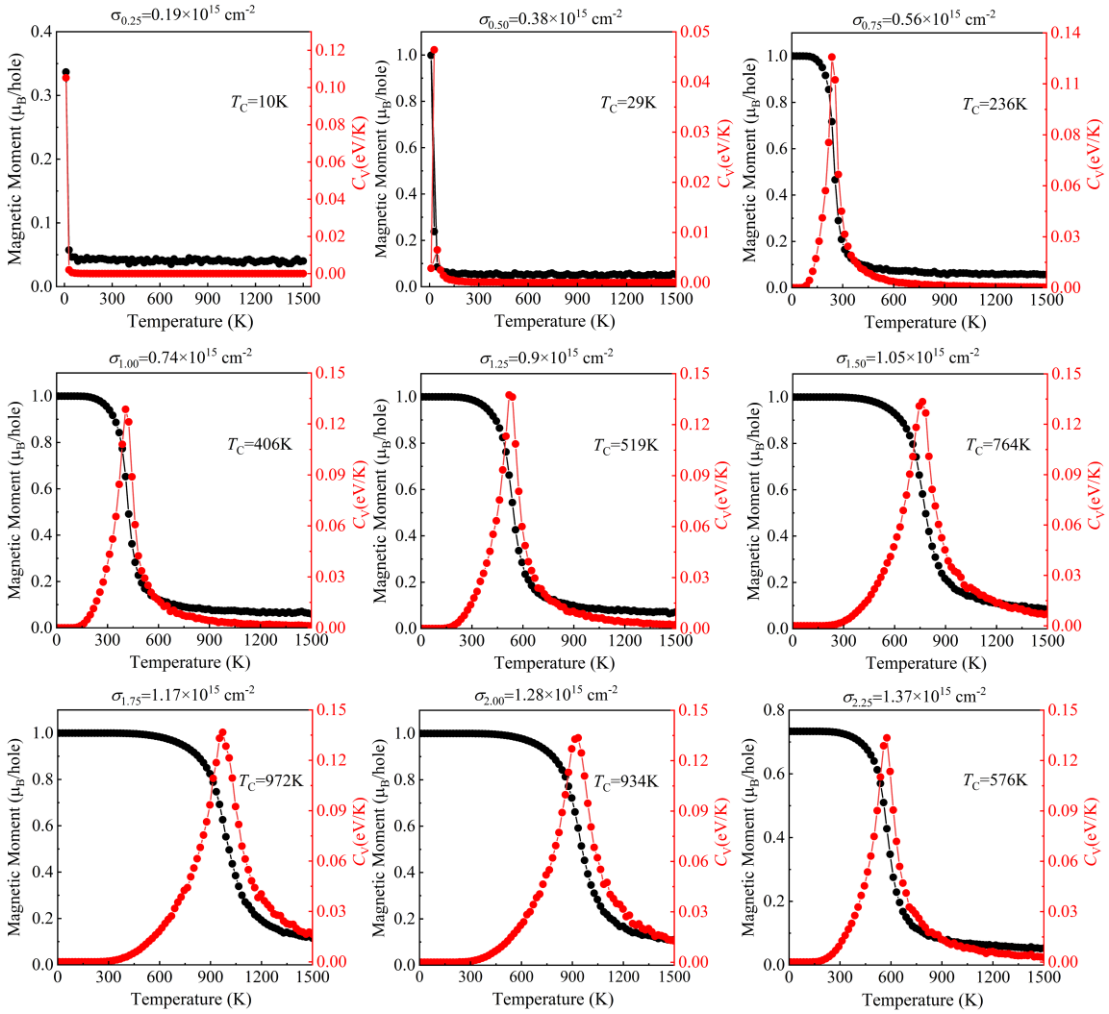

FIG. S3. The temperature-dependent magnetic moments and heat capacity (C_v) for the penta-graphene at different hole densities.

IV. Electronic band structures under different hole-doping densities

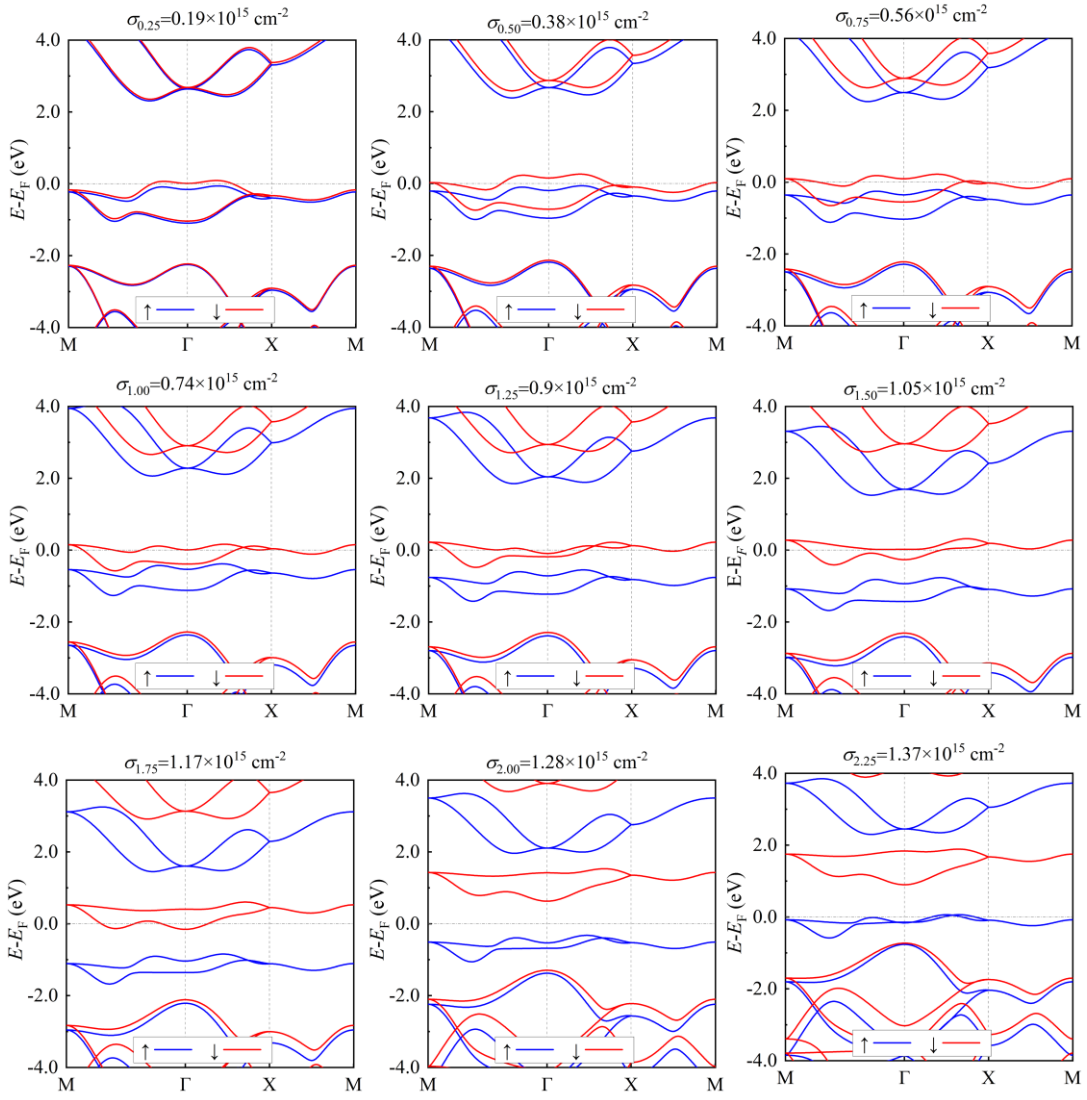

FIG. S4. The electronic band structure of penta-graphene under different hole-doping densities.

V. Electronic band structures under different biaxial strains

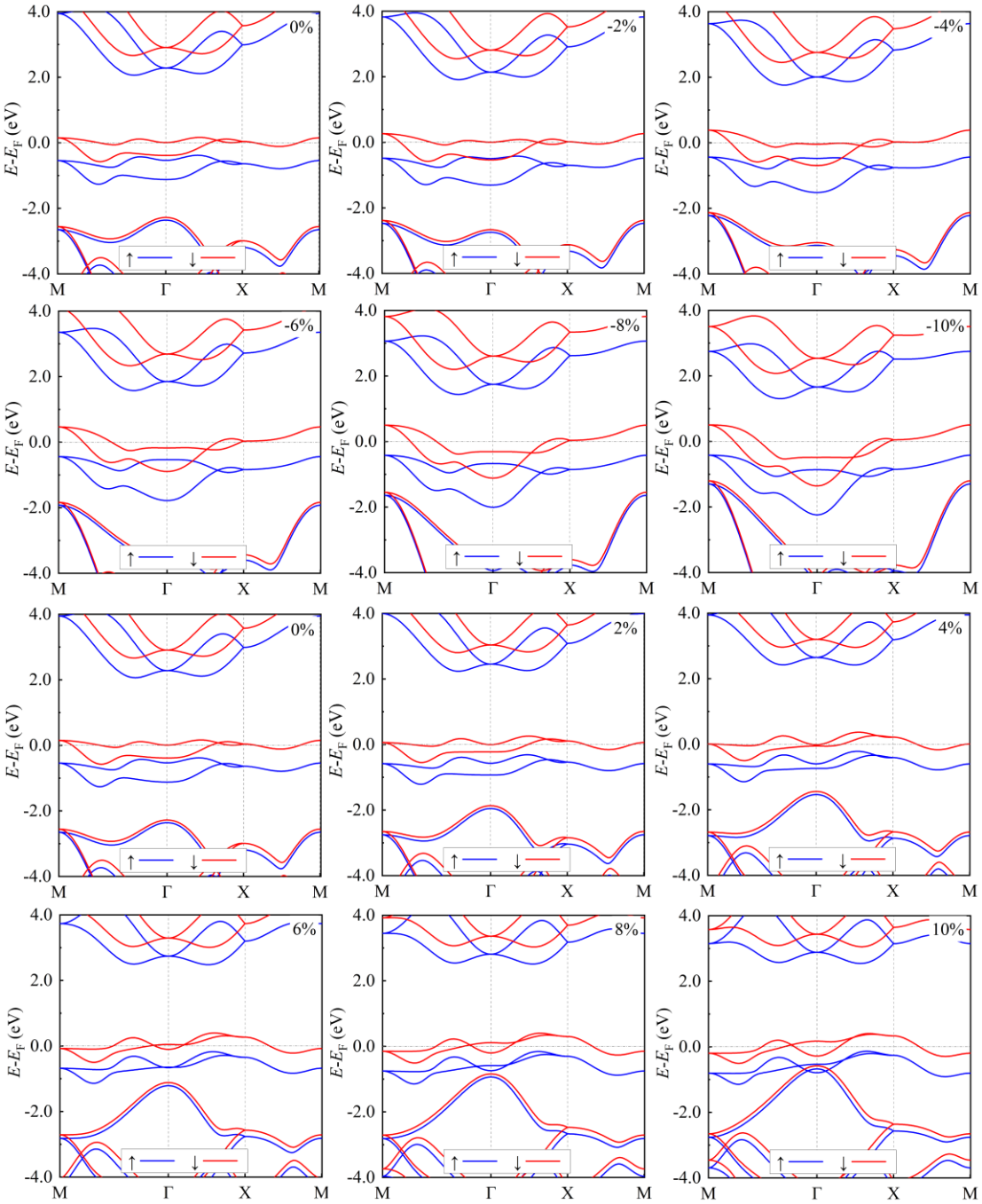

FIG. S5. Electronic band structures of penta-graphene at the density of 7.36 ×10^{14} cm^{-2} by using biaxial strains ranging from −10% to 10%.

VI. Electron transport anisotropy for the low-energy bands around W_1 and W_2

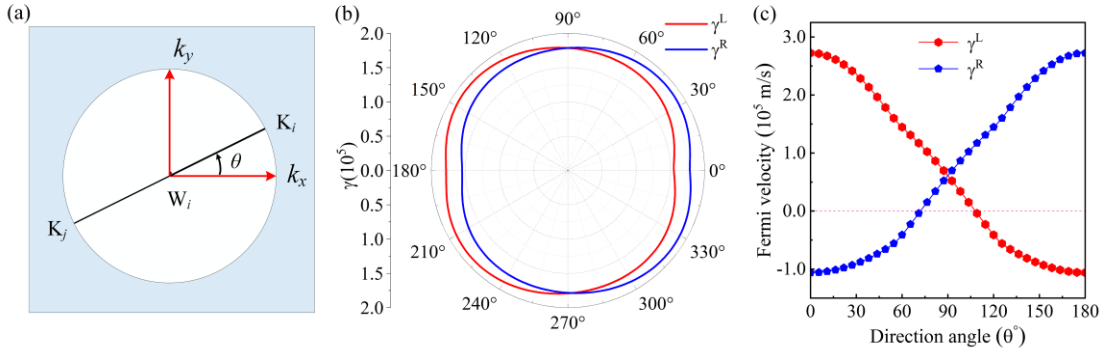

FIG. S6. (a) The schematic diagram of the polar coordinate in the 2D momentum space with the Weyl Points W_i (i = 1 and 2) as the origin. The distribution of the slope indexes γ^L and γ^R along different $\boldsymbol{k}$-directions (denoted by θ) for (b) W_1 and (c) W_2. Here, the slope index defined as $\gamma^R = v_F{}^R\mathrm{sgn}(v_F{}^L)$ and $\gamma^L = v_F{}^L\mathrm{sgn}(v_F{}^R)$. The L and R indicate the two Weyl bands, including left (L) and right (R) bands; v_F represents Fermi velocity for the corresponding linear bands, which can be evaluated from the equation of $\hbar v_F = dE(\boldsymbol{k})/\mathrm{d}\boldsymbol{k}$.

VII. Irreducible representations for the bands around W_3

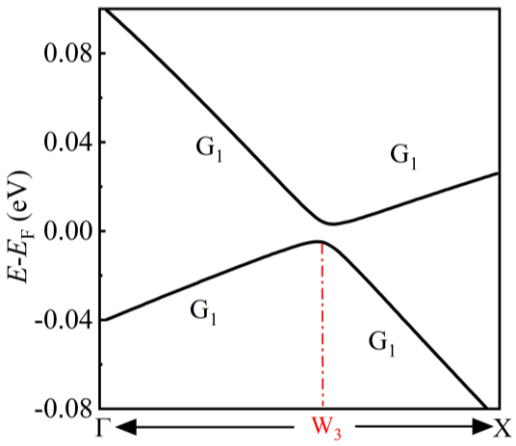

FIG. S7. Clearly, a sizable bandgap can be found at the W_3 due to the same irreducible representations, implying that there is no symmetry protection.